An Observation Linking the Origin of Plasmaspheric Hiss to Discrete Chorus Emissions

J. Bortnik, *et al.*

Science **324**, 775 (2009);
DOI: 10.1126/science.1171273

way, where adenosine diphosphate and adenosine triphosphate play the role of an activator and an inhibitor, respectively. Recent model studies (*12*) have shown that the presence of low-mobility enzymes such as phosphofructokinase can induce a short-range activation process suitable for the development of Turing patterns even when the complex is not inert.

References and Notes

1. I. R. Epstein, J. Pojman, *An Introduction to Nonlinear Chemical Dynamics* (Oxford Univ. Press, New York, 1998).
2. H. Meinhardt, *Models of Biological Pattern Formation* (Academic Press, London, 1982).
3. J. D. Murray, *Mathematical Biology* (Springer-Verlag, Berlin, 2003).
4. We do not consider the one example of transient symmetry-breaking patterns observed in a complex water-in-oil medium, which are made possible by the peculiar batch kinetic properties of the Belousov-Zhabotinsky reaction (*29*).
5. J. Boissonade, P. De Kepper, *J. Phys. Chem.* **84**, 501 (1980).
6. A. De Wit, *Adv. Chem. Phys.* **109**, 435 (1999).
7. V. Castets, E. Dulos, J. Boissonade, P. De Kepper, *Phys. Rev. Lett.* **64**, 2953 (1990).
8. K. J. Lee, W. D. McCormick, Q. Ouyang, H. L. Swinney, *Science* **261**, 192 (1993).
9. I. Lengyel, I. R. Epstein, *Proc. Natl. Acad. Sci. U.S.A.* **89**, 3977 (1992).
10. I. Szalai, P. De Kepper, *Chaos* **18**, 026105 (2008).
11. A. Turing, *Philos. Trans. R. Soc.* **237**, 37 (1952).
12. D. E. Strier, S. Ponce Dawson, *PLoS One* **2**, e1053 (2007).
13. J. E. Pearson, W. J. Bruno, *Chaos* **2**, 513 (1992).
14. P. Blanchedeau, J. Boissonade, P. De Kepper, *Physica D* **147**, 283 (2000).
15. J. Boissonade, E. Dulos, F. Gauffre, M. N. Kuperman, P. De Kepper, *Faraday Discuss. Chem. Soc.* **120**, 353 (2002).
16. I. Szalai, P. De Kepper, *J. Phys. Chem. A* **108**, 5315 (2004).
17. I. Szalai, P. De Kepper, *Phys. Chem. Chem. Phys.* **8**, 1105 (2006).
18. Z. Virányi, I. Szalai, J. Boissonade, P. De Kepper, *J. Phys. Chem. A* **111**, 8090 (2007).
19. Materials and methods are available as supporting material on *Science* Online.
20. B. Rudovics *et al.*, *J. Phys. Chem. A* **103**, 1790 (1999).
21. D. Horváth, Á. Tóth, *J. Chem. Soc. Faraday Trans.* **93**, 4301 (1997).
22. A. Hagberg, E. Meron, *Chaos* **4**, 477 (1994).
23. No stationary patterns could be obtained in the chlorite-tetrathionate (*15*) and chlorine dioxide–iodide (*16*) reactions, which do not have such an independent source or sink for the respective activatory species. Large amounts of polyacrylate or poly(vinyl alcohol) eventually induce morphological traveling front instabilities, but they have never led to a stationary pattern.
24. D. E. Strier, P. De Kepper, J. Boissonade, *J. Phys. Chem. A* **109**, 1357 (2005).
25. K. Benyaich, thesis, Université Libre de Bruxelles, Bruxelles, Belgique (2005).
26. G. Rábai, Z. V. Nagy, M. T. Beck, *React. Kinet. Catal. Lett.* **33**, 23 (1987).
27. The $[]_0$ notation denotes the concentration that the input species would have in the input flow after mixing and before any reaction.
28. R. J. Field, E. Kőrös, R. M. Noyes, *J. Am. Chem. Soc.* **94**, 8649 (1972).
29. V. Vanag, I. R. Epstein, *Chaos* **15**, 047510 (2005).

30. We acknowledge the support from the French Agence National de la Recherche, the French-Hungarian Centre Nationale de la Recherche Scientifique–Magyar Tudományos Akadémia collaboration program (21420), and the Hungarian funds Országos Tudományos Kutatási Alapprogram (49666 and 67701). I.S. thanks the support of the Bolyai Fellowship. We thank J. Boissonade and P. Borckmans for fruitful discussions.

Supporting Online Material

www.sciencemag.org/cgi/content/full/324/5928/772/DC1
Materials and Methods
Figs. S1 and S2
References

18 December 2008; accepted 16 March 2009
10.1126/science.1169973

An Observation Linking the Origin of Plasmaspheric Hiss to Discrete Chorus Emissions

J. Bortnik,[1]* W. Li,[1] R. M. Thorne,[1] V. Angelopoulos,[2] C. Cully,[3] J. Bonnell,[4] O. Le Contel,[5] A. Roux[5]

A long-standing problem in the field of space physics has been the origin of plasmaspheric hiss, a naturally occurring electromagnetic wave in the high-density plasmasphere (roughly within 20,000 kilometers of Earth) that is known to remove the high-energy Van Allen Belt electrons that pose a threat to satellites and astronauts. A recent theory tied the origin of plasmaspheric hiss to a seemingly different wave in the outer magnetosphere, but this theory was difficult to test because of a challenging set of observational requirements. Here we report on the experimental verification of the theory, made with a five-satellite NASA mission. This confirmation will allow modeling of plasmaspheric hiss and its effects on the high-energy radiation environment.

Naturally occurring electromagnetic waves are known to play a dominant role in the dynamics of Earth's radiation belts, a zone of high-energy electrons that are trapped by Earth's magnetic field (*1*–*5*). One important class of such waves is plasmaspheric hiss (*6*, *7*), which is responsible for creating a relatively empty zone, called the slot region, between the inner and outer belts, thus shaping the large-scale structure of the radiation belts (*3*, *4*). This incoherent band of waves was discovered in the late 1960s (*8*–*11*), spans from ~200 Hz to 2 kHz, and was named plasmaspheric hiss because of its confinement within the high-density plasmasphere, and its unstructured "hissy" nature. Despite the recognized importance of plasmaspheric hiss, its origin has proven remarkably difficult to identify. Here we describe an experimental observation that unambiguously links plasmaspheric hiss to a different and seemingly unrelated wave type, called chorus, occurring in distant regions of the magnetosphere.

Unlike plasmaspheric hiss, chorus occurs outside the plasmasphere as short (~0.1-s) coherent pulses in the frequency range from 0.1 f_{ce} to 0.6 f_{ce} (where f_{ce} is the frequency with which electrons gyrate about Earth's magnetic field line and is proportional to the magnetic field intensity) (*12*–*15*). Recent modeling shows that a fraction of chorus energy can propagate from its equatorial source region to high latitudes, avoid Landau damping, and refract into the plasmasphere, where it merges into the incoherent band of hiss (*7*). To do so, the chorus waves must originate from a spatial region between $L \sim 4$ and 7 (where the L value roughly tags a certain magnetic field line by the radial distance in Earth radii of its equatorial crossing), in the lower range of frequencies (~0.1 f_{ce} to 0.3 f_{ce}), with wave normals pointed toward lower L ($\psi_0 \sim -30°$ to $-60°$, where ψ_0 is the angle formed between the wave vector **k**, normal to the plane of the wave, and Earth's magnetic field). The predictions of this model are consistent with previously reported statistical observations of hiss, but a direct experimental test is challenging, because it requires simultaneous observations with at least two satellites equipped with high-resolution wave instruments capable of unambiguously detecting chorus and hiss: one located near the equatorial source region of chorus and the other in the plasmasphere, at approximately the same local time (which should coincide with the local time in which chorus and hiss both occur) and in the same frequency band, during geomagnetically active conditions. Such an experimental situation was serendipitously achieved with NASA's five-satellite THEMIS (Time History of Events and Macroscale Interactions during Substorms) mission (*16*).

At ~04:00 UT on 4 October 2008, THEMIS E was located on the day side, in the low-density region outside the plasmasphere (Fig. 1C), and was observing waves with both electric and magnetic components (Fig. 1, A and B), which were in the range from ~0.1 f_{ce} to 0.6 f_{ce} and thus consistent with chorus. Simultaneously, THEMIS D

[1]Department of Atmospheric and Oceanic Sciences, University of California, Los Angeles, CA 90095, USA. [2]Institute of Geophysics and Planetary Physics/Earth and Space Sciences, University of California, Los Angeles, CA 90095, USA. [3]Swedish Institute of Space Physics, Box 537, SE-751 21, Uppsala, Sweden. [4]Space Science Laboratory, University of California, Berkeley, CA 94720, USA. [5]Centre d'Etude des Environnements Terrestre et Planétaires, Velizy, France.

*To whom correspondence should be addressed. E-mail: jbortnik@gmail.com

was located on the day side in the high-density plasmasphere and was observing electromagnetic waves (Fig. 1, D and E) in the frequency range from ~100 Hz to 1 kHz, which were not scaled to the gyrofrequency and are consistent with hiss.

Using low-resolution data, it is not possible to determine whether there exists a correlation between chorus and hiss (Fig. 1). However, in the time interval from 03:54 to 04:00 UT (gray block in Fig. 1, C and F), both satellites switched into a high-resolution burst-collection mode (*16*), revealing that the waves recorded on THEMIS E (Fig. 2A) are discrete chorus elements, in the frequency range from ~700 Hz to 2 kHz (~0.17 to 0.5 f_{ce}), with predominantly oblique wave normal angles (Fig. 2B). THEMIS D was simultaneously observing waves between a few 100 Hz and ~2 kHz, exhibiting the typical structureless *f-t* (frequency-time) signature indicative of plasmaspheric hiss (Fig. 2C).

In the most intense portion of the chorus spectrum (~0.3 f_{ce}), there is a clear correspondence between the chorus (THEMIS E) and hiss (THEMIS D) wave power (Fig. 2D), even though the two satellites are separated radially by ~3.2 R_E (R_E, Earth radius) (~20,400 km) and by ~2.9 hours in local time. Almost every chorus element (Fig. 2D, red trace) results in an increase in hiss power (blue trace), which decays away with a time constant of ~10 s. The correspondence is most evident near the beginning of the period (03:54 UT), possibly because the longitudinal separation is at a minimum [magnetic local time (MLT) difference, ~2.78 hours] and diminishes toward the end of the period, when the longitudinal separation increases (MLT difference, ~3.05). It is possible that the ~3-hour MLT longitudinal separation between spacecraft is the maximum separation at which a correspondence between chorus and hiss can be observed, and as such this coincidental measurement is even more fortuitous. Alternatively, it is possible that the high chorus wave normals ($\psi \sim -60°$ to $-40°$) near the beginning of the period (Fig. 2B) are more conducive to producing hiss than are the lower wave normals ($\psi \sim -50°$ to $-10°$) in the later part. The average power levels of chorus and hiss are comparable (especially in the earlier part of the observation), but the hiss intensity is weaker than that of the individual chorus elements by a factor of ~100. The results of a frequency-resolved cross-covariance analysis (Fig. 3) indicate that the correlation is strongest [correlation coefficient (r) ~ 0.7] in the most intense spectral portion of the chorus (~1200 to 1650 Hz) and occurs when the hiss waveform lags behind the chorus waveform by ~1 to 7 s. The intense hiss spectrum at ~100 to 700 Hz (Fig. 2C) is expected to be generated by chorus at $L > 6$ (that is, regions of lower f_{ce}), as suggested in Fig. 1.

Theoretical analysis similar to that of (*7*) showed that a group of rays representing chorus, initiated near the location of THEMIS E ($L = 6$), was able to propagate into the plasmasphere and be observed near the location of THEMIS D ($L = 2.8$) (Fig. 4). The key angular range of rays that entered the plasmasphere and evolved into plasmaspheric hiss was $\psi_0 \sim -49.5°$ to $-46.5°$ (similar to the measured angles in Fig. 2B), with waves at $\psi_0 < -50°$ becoming Landau-damped before reaching the plasmasphere, and waves with $\psi_0 > -46°$ being unable to refract into the plasmasphere and instead propagating to the ground (Fig. 4A, green and yellow rays) or refracting toward higher L shells (red rays) and possibly forming a different emission called extremely low-frequency (ELF) hiss (*17*).

To further quantify the approximate time scale of chorus entry into the plasmasphere, we traced a single ray for its entire lifetime (Fig. 4B), from initiation at $t = 0$ s to termination at $t = 20$ s. Using

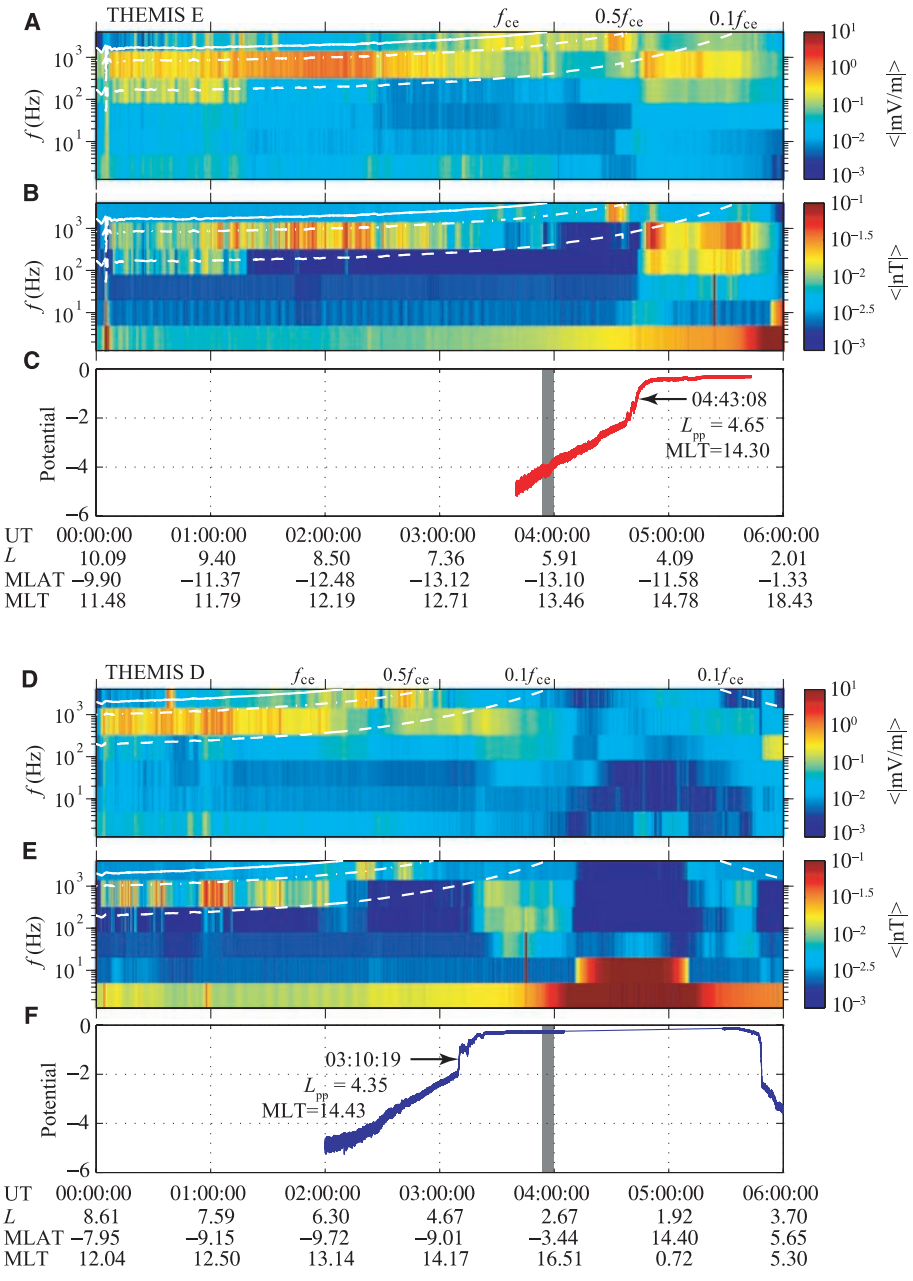

Fig. 1. A 6-hour overview plot of simultaneous data recorded by THEMIS E [(A) to (C)] and THEMIS D [(D) to (F)] on 4 October 2008. (**A** and **D**) The wave electric field intensity and (**B** and **E**) the wave magnetic field intensity in six frequency bins from 2 Hz to 4 kHz. (**C** and **F**) The spacecraft electric potential, which acts as a proxy for the electron density. The *x* axis labels indicate each satellite's universal time (UT) local *L* value; the magnetic latitude (MLAT), which is the latitude of each spacecraft relative to the geomagnetic equator; and MLT, which is the local time of the equatorial crossing of the magnetic field line passing through the satellite and can be slightly different from the actual local time. The white lines in (A) and (B) and (D) and (E) represent fractions of the equatorial gyrofrequency (f_{ce}) corresponding to 1, 0.5, and 0.1, represented by solid, dash-dotted, and dashed lines, respectively. The inferred plasmapause crossing based on spacecraft potential is shown in (C) and (F). The magnetic signal <20 Hz [(B) and (E)] at low *L* is due to contamination from Earth's geomagnetic field.

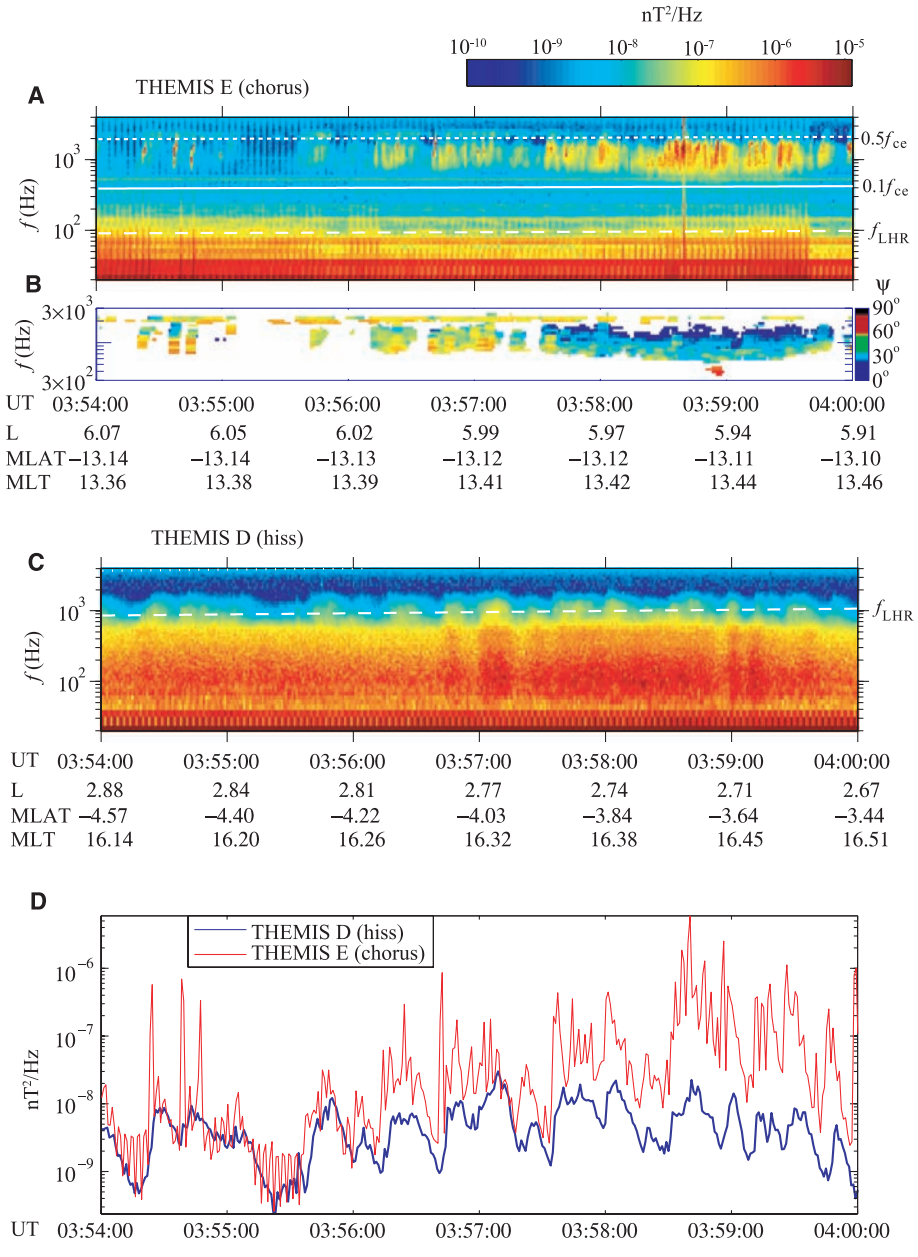

Fig. 2. High-resolution data from the two THEMIS spacecraft from 03:54 to 04:00 UT, corresponding to Fig. 1. (**A**) Wave magnetic field data recorded by THEMIS E, in the range from 20 Hz to 4 kHz. (**B**) Corresponding wave normal angle estimates of the intense chorus elements in the range from 300 Hz to 3 kHz, calculated using (*19*). (**C**) THEMIS D data shown as in (A). (**D**) Frequency-averaged magnetic field intensity in the frequency band from 1200 to 1650 Hz, for THEMIS E (red trace) and D (blue trace). The ephemeris of each spacecraft is shown on the *x* axes of (A) and (C) in the same format as Fig. 1. The white dashed line in (A) and (C) corresponds to the local lower hybrid resonance frequency (f_{LHR}); the white solid and dotted lines in (A) are 0.1 and 0.5 f_{ce}, respectively; and signals below ~200 Hz suffer from instrumental noise. High-resolution wave electric field data corresponding to (A) and (B) were also recorded by THEMIS E and D and look similar to the magnetic field data (not shown in the figure).

this representative ray, we found that the ray entered the plasmasphere at approximately $t = 1$ s and crossed the geomagnetic equator at $t = 2$ s, near $L = 3$. This is in agreement with observations by THEMIS D (Fig. 2), which was located at $L \sim 2.8$ during the period of hiss observation and according to our model would have recorded the first entry of the chorus wave power at roughly $t \sim 2$ s after chorus was excited. The ray then continued to propagate and filled the entire plasmasphere (Fig. 4B, solid gray oval). It experienced a magnetospheric reflection at $t \sim 3$ s, reflected off the plasmapause at $t \sim 4.5$ s, and recirculated back to lower L. At $t \sim 7.5$ s, the ray returned again to the geomagnetic equator, at $L \sim 2.5$, and would have been sensed again by a satellite at that location. Thereafter, the ray continued to propagate and was completely damped at $t = 20$ s. The relevant time scales for observing chorus wave power appearing inside

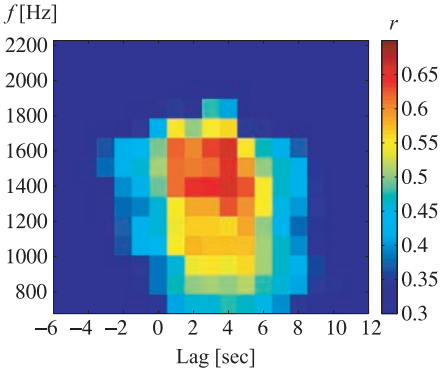

Fig. 3. Cross-covariance analysis between THEMIS E and D data. A frequency-resolved cross-covariance analysis in 16 frequency channels between 700 Hz and 2.2 kHz is shown as a function of time lag, positive values indicating that THEMIS D data (hiss) lags behind THEMIS E data (chorus). The time-series data are taken from the first 3 min (03:54 to 03:57 UT) of the wave magnetic intensity in Fig. 2, A and B, because this gives slightly more resolved time lags than would using the entire 6-min interval. The time series in each frequency band is normalized so that the autocovariance is 1 at zero lag.

the plasmasphere and propagating multiple times across the equator in the vicinity of $L \sim 2.8$ is $t \sim 2$ to 7 s for the entire group of rays shown in Fig. 4A. Comparing Fig. 4B to Fig. 3, the peak correlation between the hiss and chorus waveforms occurs with a ~2- to 7-s lag, in direct agreement with the theory.

The high-resolution observation made by the THEMIS satellites directly supports the theory of the origin of plasmaspheric hiss, which involves

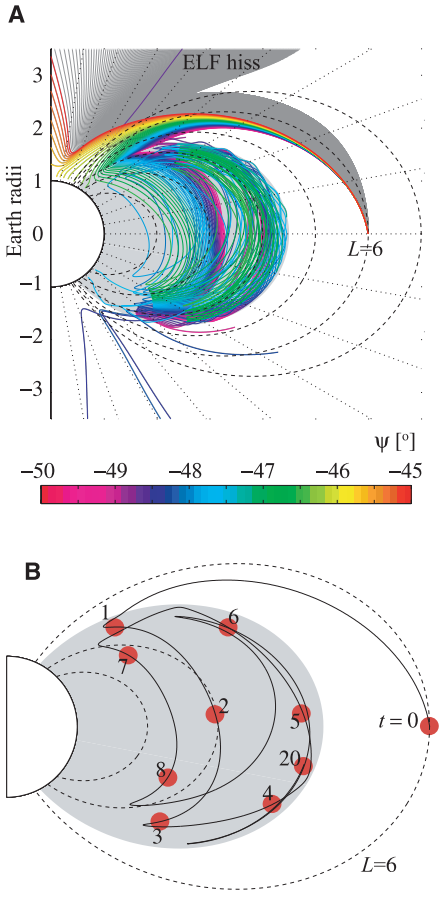

Fig. 4. Ray-tracing model of chorus and hiss. (**A**) Ray paths representing chorus are initiated at the equator, at $L = 6$, $f = 0.21\ f_{ce}$ (~855 Hz), in the range $\psi_0 = -50°$ to 0° (gray ray paths), plotted at every 0.1°, with the key wave normal range $\psi_0 = -50°$ to −45° that enters the plasmasphere shown in color. The corresponding color scale indicates the initial wave normal angle of each ray in degrees. (**B**) A single ray from the group shown in (A) is displayed, with $\psi_0 = -48°$. The red circles indicate group time in seconds, from the time of ray initiation $t = 0$ s. The day-side cold plasma density is modeled according to (*20*), with the plasmapause located at $L = 4.5$, for consistency with the THEMIS observations; and the L-dependent suprathermal flux model was used as in (*7*, *21*) for active conditions. Each ray in (A) and (B) is plotted only while its power is above 1% of its initial value, so that in the case of (B), the ray duration is ~20 s.

the propagation and evolution of discrete chorus elements from their source region outside the plasmasphere into the incoherent noise band that characterizes plasmaspheric hiss, inside the plasmasphere. Understanding the origin of hiss will enable space physicists to calculate spatial maps of hiss characteristics and in turn predict the effect of hiss on the radiation belt electrons that are a known hazard to astronauts and to a variety of technological systems in space (*18*).

References and Notes

1. C. F. Kennel, H. E. Petschek, *J. Geophys. Res.* **71**, 1 (1966).
2. L. R. Lyons, R. M. Thorne, C. F. Kennel, *J. Geophys. Res.* **77**, 3455 (1972).
3. R. W. Abel, R. M. Thorne, *J. Geophys. Res.* **103**, 2385 (1998).
4. L. R. Lyons, R. M. Thorne, *J. Geophys. Res.* **78**, 2142 (1973).
5. R. B. Horne *et al.*, *J. Geophys. Res.* **111**, A03225 (2005).
6. R. M. Thorne, E. J. Smith, R. K. Burton, R. E. Holzer, *J. Geophys. Res.* **78**, 1581 (1973).
7. J. Bortnik, R. M. Thorne, N. P. Meredith, *Nature* **452**, 62 (2008).
8. N. Dunckel, R. A. Helliwell, *J. Geophys. Res.* **74**, 6371 (1969).
9. C. T. Russell, R. E. Holzer, E. J. Smith, *J. Geophys. Res.* **74**, 755 (1969).
10. W. W. L. Taylor, D. A. Gurnett, *J. Geophys. Res.* **73**, 5615 (1968).
11. M. Hayakawa, S. S. Sazhin, *Planet. Space Sci.* **40**, 1325 (1992).
12. R. K. Burton, R. E. Holzer, *J. Geophys. Res.* **79**, 1014 (1974).
13. W. J. Burtis, R. A. Helliwell, *Planet. Space Sci.* **24**, 1007 (1976).
14. S. S. Sazhin, M. Hayakawa, *Planet. Space Sci.* **40**, 681 (1992).
15. O. Santolik, *Nonlinear Process. Geophys.* **15**, 621 (2008).
16. V. Angelopoulos, *Space Sci. Rev.* **141**, 5 (2008).
17. O. Santolik *et al.*, *J. Geophys. Res.* **111**, A10208 (2006).
18. D. N. Baker, *Science* **297**, 1487 (2002).
19. D. Lengyel-Frey *et al.*, *J. Geophys. Res.* **99**, 13325 (1994).
20. D. L. Carpenter, R. R. Anderson, *J. Geophys. Res.* **97**, 1097 (1992).
21. J. Bortnik, R. M. Thorne, N. P. Meredith, *J. Geophys. Res.* **112**, A08204 (2007).

22. The authors gratefully acknowledge support from NASA grant NNX08A1135G and contract NAS5-02099.

22 January 2009; accepted 31 March 2009
10.1126/science.1171273

The Role of Aerosols in the Evolution of Tropical North Atlantic Ocean Temperature Anomalies

Amato T. Evan,[1,2]* Daniel J. Vimont,[2] Andrew K. Heidinger,[3] James P. Kossin,[4] Ralf Bennartz[2]

Observations and models show that northern tropical Atlantic surface temperatures are sensitive to regional changes in stratospheric volcanic and tropospheric mineral aerosols. However, it is unknown whether the temporal variability of these aerosols is a key factor in the evolution of ocean temperature anomalies. We used a simple physical model, incorporating 26 years of satellite data, to estimate the temperature response of the ocean mixed layer to changes in aerosol loadings. Our results suggest that the mixed layer's response to regional variability in aerosols accounts for 69% of the recent upward trend, and 67% of the detrended and 5-year low pass–filtered variance, in northern tropical Atlantic Ocean temperatures.

Since 1980, tropical North Atlantic Ocean temperatures have been rising at a rate of nearly 0.25°C per decade (*1*). Studies have attributed this increase, explicitly and implicitly, to global warming (*2*, *3*), mean Northern Hemisphere temperature variations (*4*), changes in the thermohaline circulation (*5*, *6*), or some combination of these factors (*7*). However, many of these studies fail to provide either a mechanism for or direct evidence of how these variables control tropical North Atlantic Ocean temperatures. At the same time, models (*8*) and observations (*1*, *9*) demonstrate that local changes in aerosol cover should have a non-negligible impact on Atlantic Ocean temperature via the scattering of sunlight and reduction in surface solar insolation.

The tropical North Atlantic is unique among tropical ocean basins because of its oftentimes extensive and heavy aerosol cover (*10*), a consequence of being downwind of West Africa, the world's largest dust source (*11*). Annual North African dust emission and deposition to the North Atlantic have been estimated to be 240 to 1600 Tg and 140 to 259 Tg, respectively (*12*), with the peak in West African dust production occurring during the boreal summer months (*13*). A smoothed time series of northern tropical Atlantic dust cover (Fig. 1) shows a maximum and minimum in dust activity that occurred in 1985 and 2005, respectively, and a downward trend in dust optical depth over the record. It has been shown that during both the summer (*14*) and winter seasons (*15*) these year-to-year changes

[1]Cooperative Institute for Meteorological Satellite Studies, University of Wisconsin, Madison, WI 53706, USA. [2]Department of Atmospheric and Oceanic Sciences, University of Wisconsin, Madison, WI 53706, USA. [3]National Oceanic and Atmospheric Administration (NOAA)/National Environmental Satellite, Data, and Information Service (NESDIS)/Center for Satellite Applications and Research (STAR), 1225 West Dayton Street, Madison, WI 53706, USA. [4]NOAA/NESDIS/National Climatic Data Center, Madison, WI 53706, USA.

*To whom correspondence should be addressed. E-mail: atevan@wisc.edu